Mathematical Modeling of Hydraulic Fracturing

In Shale Gas Reservoirs

by

Ali Sadaghiani Zadeh

15217

Dissertation submitted in partial fulfillment of
The requirements for the
Bachelor of Engineering (Hons)
(Petroleum)

MAY 2014

Universiti Teknologi PETRONAS
Bandar Seri Iskandar
31750 Tronoh
Perak Darul Ridzuan

CERTIFICATION OF ORIGINALITY

This is to certify that I am responsible for the work submitted in this project, that the original work is my own except as specified in the references and acknowledgements, and that the original work contained herein have not been undertaken or done by unspecified sources or persons.

_____

ALI SADAGHIANI ZADEH

ABSTRACT

During the past few years, hydraulic fracturing and horizontal drilling have facilitated the production of gas from shale reserves that were uneconomic to produce in the past. Each shale formation has a specific nature, therefore every basin or well may need to be treated differently. Additionally, shales have characteristics such as extremely low permeability, sensitivity to contacting fluids, and existing micro fractures which cause complications while evaluating them. There is also an absence of a clear explanation for the application of 2D models and the effect of various parameters on the fracture in shale formations. Therefore, the objective of this study is to analyze different 2D hydraulic fracture geometry models while examining these models for their application in shale gas formations and to identify a 2D model that is most suitable to be used in the hydraulic fracture treatment design of shale gas reservoirs. It is also intended to investigate the effect of fracture height, fluid loss and rock stiffness on the fracture geometry and the well.

In this study the two most commonly used hydraulic fracture geometry models in the oil and gas industry, PKN and KGD, have been discussed and based on these models two mathematical computer codes were developed in order to calculate various parameters such as fracture length, average fracture width, wellbore net pressure, pumping time, and maximum fracture width at wellbore. The PKN-C model is identified as the most suitable 2D model to be used in shale gas reservoirs due to its more acceptable vertical plane strain assumption. Low permeability formations such as shale reservoirs require narrower and longer fractures for a higher productivity. Thus, using a model that would predict longer and narrower fractures, such as the PKN-C model, would be more suitable. The KGD-C model predicts a higher dimensionless fracture conductivity compared to the PKN-C model. However, the fracture geometry predicted by the PKN-C model results in higher post-fracture productivity. Additionally, it was observed that longer and narrower fractures are produced in rocks with a high Young's modulus (such as shale). Additionally, increasing the leak off coefficient when fluid loss is small will result in slightly shorter fracture lengths, while increasing the leak off coefficients when fluid loss is high will result in significantly shorter fracture lengths.

Acknowledgment

I would like to deliver my deepest gratitude and appreciation to my advisor, Mr. Mohammad Amin Shoushtari, for his support and guidance throughout the completion of this project. I also wish to express my gratitude to the faculty of Petroleum Engineering and all lecturers for making my stay at Universiti Teknologi PETRONAS a great experience.

I would also like to thank my friends, Including Payam, Sahar, and Behnaz for their help while developing the mathematical code in this project. I thank my brother, Mohammad, my consistent source of consultation and support during all steps of my study. I especially thank my father and mother for all they have done for me in all these years and for all that they have provided me with to see this day.

Finally I thank my lovely wife for her patience, encouragement, and unending support throughout my study and for standing by me through all my absences. She has certainly been my motivation for continuing to improve.

TABLE OF CONTENTS

LIST OF TABLES

LIST OF FIGURES

NOMENCLATURE

A	Fracture surface area
C_L	Leak off coefficient
E	Young's modulus
E'	Plane strain modulus
F_{CD}	Dimensionless fracture conductivity
FOI	Folds of increase
$K_f w$	Fracture conductivity
$p_{n,w}$	Wellbore net pressure
S_p	Spurt loss
h_f	Fracture height
i	Injection rate
k	Reservoir permeability
k_f	Fracture permeability
r_e	Drainage radius
r_w	Wellbore radius
r'_w	Equivalent wellbore radius
s	Skin factor
t	Injection time
$w_{w,0}$	Maximum fracture width at wellbore
x_f	Fracture half-length
β	Auxiliary variable for Carter II equation
η	Fluid Efficiency
μ	Viscosity

CHAPTER 1

INTRODUCTION

1.1 Background

Unconventional Shale formations are fine-grained, organic-rich, sedimentary rocks. Shales can contain valuable sources of oil and/or gas. However, these fine grained sedimentary rocks have some specific characteristics that cause complications while evaluating them. Some of these important characteristics are the extremely low permeability of shales, sensitivity to contacting fluids, and existing micro fractures. Thus, due to shales extremely low pore sizes and low permeability, the formation is resistant to hydrocarbon flow unless natural or artificial fractures occur.

Therefore, According to Gomaa et. al. (2014), the most important factor in developing unconventional formations is increasing the contact of fracture surface area and formation with horizontal drilling and fracturing practices. In other words, the aim is to increase the fracture surface area to obtain best results. Hence, maximizing the fracture complexity is one of the major goals in designing the shale fracture treatment.

Hydraulic fracturing is one of the major techniques that has made the economic production of natural gas from shale reservoirs possible. Hydraulic fracturing can be defined as the procedure of injecting a fluid at a pressure and flow rate that the fluid is unable to escape into the formation. This will eventually cause the wellbore to split along its axis. (Valko and Economides, 1995).

During the past few years, hydraulic fracturing and horizontal drilling have facilitated the production of oil and gas from shale reserves that were uneconomic to

produce in the past (Gomaa et. al. 2014). According to the American Petroleum Institute (2013), hydraulic fracturing will make up for almost 75% of natural gas development in the years to come, and in its absence, USA's domestic natural gas and oil production would be reduced by 45% and 17% respectively within five years.

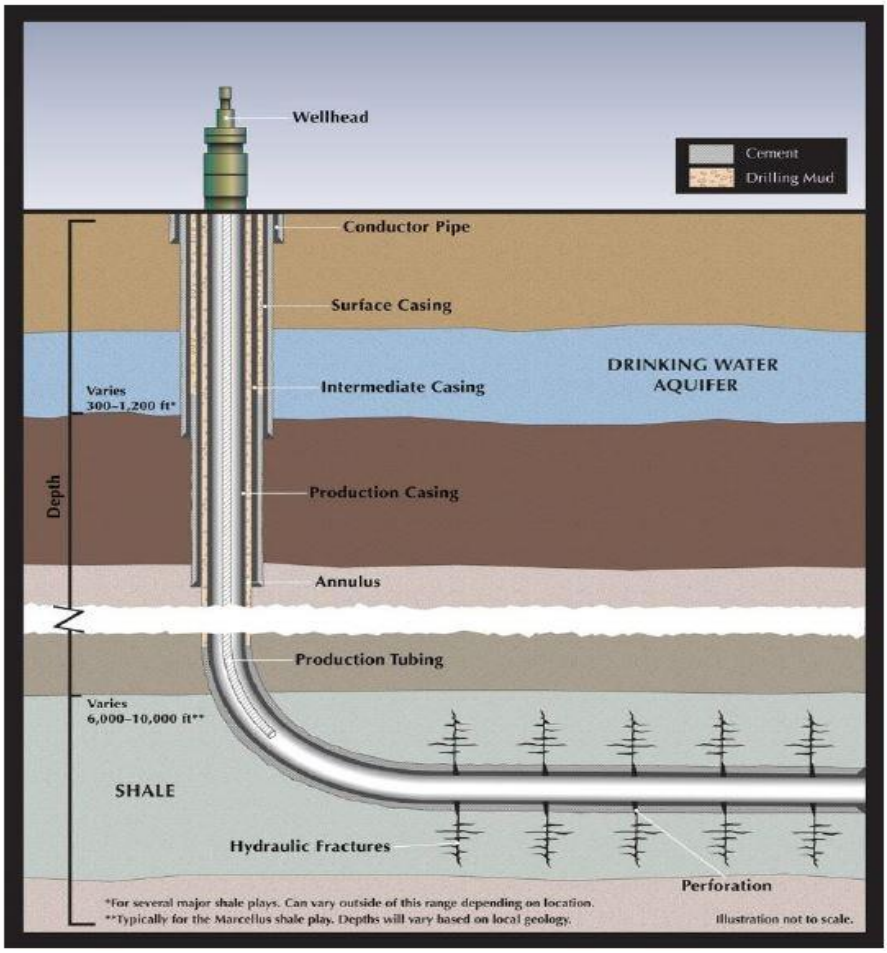

Figure 1.1 Hydraulic fracturing. Adapted from Hydraulic Fracturing and Shale Gas Production (p. 2), by C. Clark et al., 2013, Argonne National Laboratory.

As in many cases the successful production of a well depends on a successful hydraulic fracture treatment. Therefore, it is vital to be able to predict the fracture geometry growth and drainage volumes according to treatment parameters. Previously, several 2D and 3D models have been developed to determine the fracture geometry. Among these models, two of them have been mostly used in the petroleum industry and are commonly known as KGD and PKN.

Economides and Nolte (1989) expressed four main reasons for developing and using hydraulic fracturing models:

> *• perform economic optimization (determine what size treatment provides the highest rate of Return on investment) • design a pump schedule • simulate the fracture geometry and proppant placement Achieved by a specified pump schedule • evaluate a treatment.*

1.2 Problem Statement

Each shale formation has a specific nature, therefore every basin or well may need to be treated differently. Additionally shales have characteristics such as extremely low permeability, sensitivity to contacting fluids, and existing micro fractures, which cause complications while evaluating them. There is also an absence of a clear explanation for the application of 2D models and their affecting parameters on the fracture in shale formations.

1.3 Objectives

The objectives of this study are:

- To study and analyze different hydraulic fracture geometry models while examining these models for their application in unconventional formations.
- To identify a two-dimensional hydraulic fracture geometry model which is most suitable to use in the hydraulic fracture treatment design for shale gas reservoirs
- To perform sensitivity analysis and investigate the effect of various parameters such as fluid leak off, fracture height, and rock stiffness on the fracture geometry and the well.

1.4 Scope of Study

In this study various two-dimensional hydraulic fracture geometry models, such as the PKN and KGD models are studied. Due to time constraints and for simplicity, only the two-dimensional models are studied and used in this research. Furthermore,

a mathematical computer code, based on the most appropriate 2D model in shale gas reservoirs, is developed and the effecting parameters of the model are investigated and analyzed. Moreover, another mathematical computer code is developed based on a second 2D model to be used in comparison and analysis of effecting parameters.

CHAPTER 2

LITERATURE REVIEW

2.1 Hydraulic Fracturing Treatment

Hydraulic fracturing is a stimulation technique that is used to increase productivity of wells by extending a conductive path into the reservoir (Economides, et al., 1989). The fracturing treatment is done in two stages. Initially, fracturing fluids are pumped into the formation at flow rates higher than the fluid is able to leak off into the formation. At this point the fluid pressure builds up and will overcome the rock's compressive stress or breakdown pressure, causing a fracture in the formation (Guo, Lyons, & Ghalambor, 2007). This stage in known as the pad stage. As long as the fluid is being injected at a rate higher than the fluid can leak off, the fracture propagates further into the formation and grows in length and width. The second stage, commonly known as the slurry stage, is carried out by adding sand or proppant to the injection fluid. The proppant with a high compressive strength is added to the injection fluid to withstand the formation stress and hold the fracture open after pumping is stopped in order to retain a conductive flow channel (Guo et al., 2007).

2.2 Hydraulic Fracturing Mechanics

According to Nolen-Hoeksema (2013), the required pressure to create a fracture, the fracture's size, and its orientation depend on three principal compressive stresses; the vertical stress or the overburden stress, and the maximum and minimum horizontal stresses (figure 2.1). Nolen-Hoeksema continues by explaining that hydraulic fractures are tensile fractures, and propagate perpendicular to the minimum compressive stress. Thus, if the smallest compressive stress is the minimum

horizontal stress, a vertical fracture is initiated and propagates parallel to maximum horizontal stress.

Usually in relaxed geological formations, the smallest stress is horizontal, thus vertical fractures are produced, and in environments with active tectonic compression, the smallest stress is vertical, thus horizontal fractures are produced.

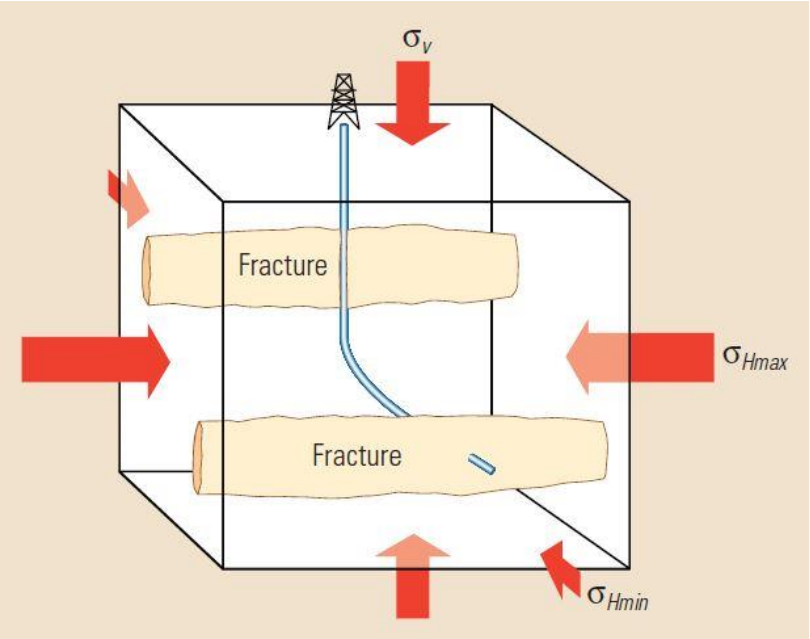

Figure 2.1 Hydraulic fracturing mechanics. Adapted from Elements Of Hydraulic Fracturing by R. Nolen-Heoksema (2013).

2.3 Two Dimensional Hydraulic Fracturing Models

Khristianovitch and Zheltov's (1959) summarized the early efforts on hydraulic fracturing modeling that was carried out by a number of researchers. Another key effort was the work performed by Perkins and Kern (1961).

The models designed by these researchers were developed in order to determine the width of the fracture for a given length and flow rate. However these models would not satisfy the volume balance (Valko et al., 1995).

Moreover, Carter (1957) presented a model which would satisfy the volume balance. In this model a constant uniform fracture width was assumed. To make sure that the width of the fracture was adequate for the proppant to enter the fracture, the model

provided more accurate width profiles compared to the previous versions and it was widely used to calculate volume balance. However with the further development of the Khristianovitch and Zheltov Model by Geertsma (1969) and Perkins & Kern model by Nordgren (1972) this method became obsolete. The two modified models, commonly known as PKN and KGD, are the first models that take account of both volume balance and solid mechanics.

2.3.1 PKN Model:

Perkin and Kern (1961) established a model to determine fracture length and width while assuming a fixed height. This model was further improved by Nordgren (1972) by considering fluid-loss in to the formation. The improved model is known as PKN. In the PKN model fracture toughness is neglected. This is because of the energy that is required for fracture propagation is considerably less compared to the energy required for the fluid to flow across the fracture's length. Additionally fracture height is fixed and propagates along the horizontal direction (figure 2.2).

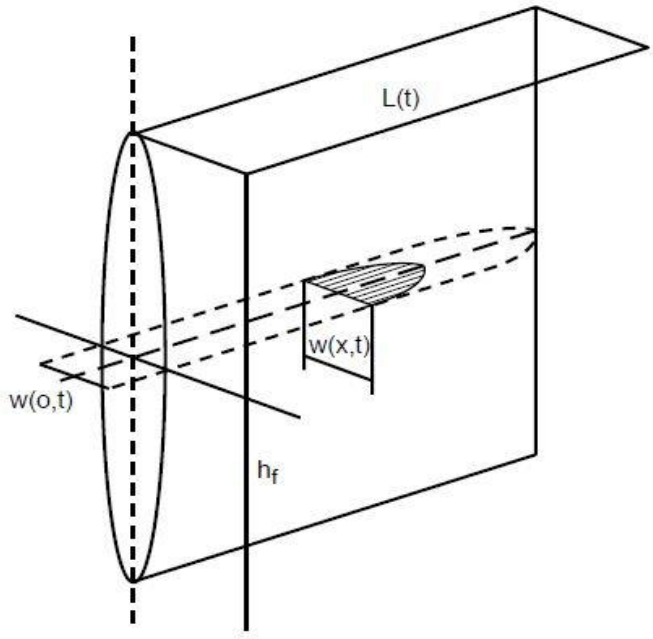

Figure 2.2 PKN fracture geometry. Adapted from Reservoir Stimulation (p. 6-4), by M. J. Economides and K. G. Nolte, 1989, Houston, TX: Schlumberger Educational Services.

The PKN model is based on the plane strain assumption and by assuming a fixed fracture height and smaller than the fracture length the problem is reduced to two dimensions. This model assumes the plane strain in the vertical direction and each vertical cross section deforms individually and is not hindered by neighboring

vertical planes. Moreover, in the PKN Model, the strains for opening or shearing the fracture are completely concentrated in vertical cross-sections and normal to the fracture's propagation direction. This can be assumed if the fracture's length is significantly greater than its height. Additionally, in this model, a constant pressure for the fracturing fluid is assumed in the vertical cross sections and normal to the direction of the fracture propagation (Gidley et al., 1989).

2.3.2 KGD Model

The KGD was initially developed by Khristianovitch and Zheltov (1955) and improved by Geertsma and de Klerk (1969). This model, again, assumes a fixed fracture height. Moreover, KGD considers the rock stiffness in the horizontal plane. Consequently, the width of the fracture will only depend on the fracture height through the boundary condition at the wellbore while assuming a constant flow rate in the fracture. In the KGD model the flow rate per unit fracture height does influence fracture width, however width is constant in the vertical direction as the plane strain is assumed to be in the horizontal direction (figure 2.3). As a result, horizontal cross sections deform individually. This can be assumed if the fracture's length is significantly shorter than its height.

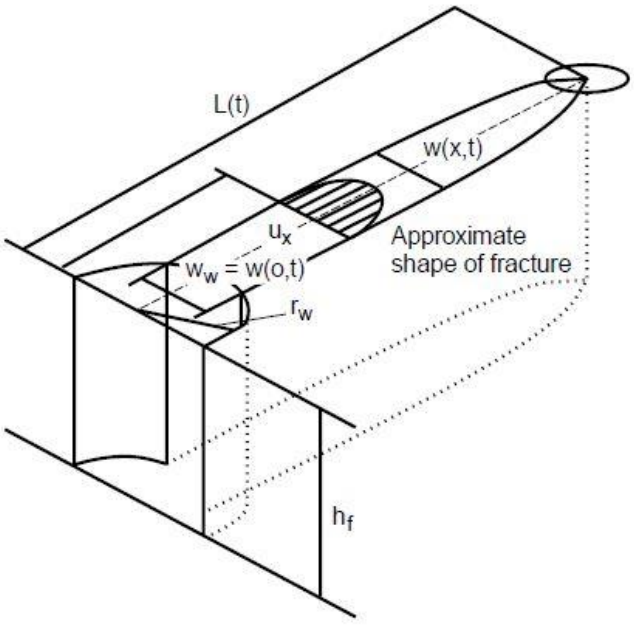

Figure 2.3 KGD Fracture Geometry. Adapted from *Reservoir Stimulation* (p. 6-4), by M. J. Economides and K. G. Nolte, 1989, Houston, TX: Schlumberger Educational Services.

Below are the six assumptions of the KGD model summarized by J. Xiang (2011):

> *"**1**-The fracture has an elliptical cross section in the horizontal plane -**2**- each horizontal plane deforms independently -**3**- fracture height, hf , is constant -**4**-fluid pressure in the propagation direction is determined by flow resistance in a narrow rectangular, vertical slit of variable width -**5**- fluid does not flow through the entire fracture length -**6**- cross sections in the vertical plane are rectangular (fracture width is constant along its height) (Geertsma and Klerk 1969)."*

2.3.3 PKN-C Model

Valko et al. (1995) claimed that a significant portion of the oil & gas engineering work have concluded that Perkins-Kern's width equation is inaccurate to some degree and an improved constant is employed instead:

$$w_{w,0} = 3.27\left(\frac{\mu i x_f}{E'}\right)^{1/4} \qquad \textbf{(2.1)}$$

Where $w_{w,0}$ is the Maximum width, μ is fluid viscosity, i is the injection rate, x_f is the fracture length, and E' is the plane strain modulus

In the equation above the constant 3.27 is derived from a limiting result of Nordgren. The average width is also expressed as:

$$\overline{w} = \frac{\pi}{5} w_{w,0} = 2.05\left(\frac{\mu i x_f}{E'}\right)^{1/4} \qquad \textbf{(2.2)}$$

Where $\overline{w}$ is the average fracture width.

The -C- used in the name of this model is to indicate the usage of the Carter-II equation.

Carter claimed that the sum of fluid leak-off rates and rate of volume growth in the produced fractures is equivalent to the injection rate entering one wing of the fracture.

The Carter-II equation is expressed as:

$$i = 2\int_0^t \frac{C_L}{\sqrt{t-\tau}} \frac{dA}{dt} d\tau + (w + 2S_p)\frac{dA}{dt} + A\frac{dw}{dt} \quad \textbf{(2.3)}$$

Moreover, the fracture length is expressed as:

$$x_f = \frac{(\overline{w} + 2S_p)i}{4{C_L}^2 \pi h_f}\left[\exp(\beta^2)erfc(\beta) + \frac{2\beta}{\sqrt{\pi}} - 1\right] \quad \textbf{(2.4)}$$

Where, $\beta = \dfrac{2C_L\sqrt{\pi t}}{\overline{w} + 2S_p}$ **(2.5)**

Where C_L is the leak off coefficient, S_p is the Spurt Loss, and h_f is the Fracture Height.

Finally the net wellbore pressure can be calculated as:

$$p_{n,w} = \frac{E'}{2h_f} w_{w,0} \quad \textbf{(2.6)}$$

2.4 The Effect of Parameters on Fracture Geometry

Gomaa et. al. (2014) conducted an experimental research in order to determine the hydraulic breakdown pressure of fractures in shales. In this research various parameters such as, injection rate, acid injection, fluid types and several additives were studied and their effect on the breakdown pressure was investigated. Furthermore the effect of parameters on fracture shape and direction were studied.

It was found that there is a strong relationship between the breakdown pressure and fracture fluid viscosity in shale formations. Gomaa concluded that a higher viscosity

results in an increase in the breakdown pressure of shale. It was further concluded that the breakdown pressure will be reduced by increasing the rate of injection and also by injecting HCL. Moreover, the results of the study indicated that a reduced fluid viscosity will result in growth of the fracture complexity.

In another research, Xiang (2011) has investigated the effect of various parameters such as shale properties, fracturing fluids and leak off rates on the geometry of the fracture. Additionally the effect of parameters on the fracture pressure has been examined.

Xiang (2011) concluded in his research that using high fluid viscosities will result in shorter and wider fractures while employing fluids with lower viscosities will result in narrower and longer fractures. The research also argues that in soft formations with a small shear modulus, shorter and wider fractures are produced while in a hard formation with a greater shear modulus, longer and narrower fractures are generated. Additionally it was found that reducing the leak off coefficient will result in the increased values of width, length and closure time of the fracture.

CHAPTER 3

METHODOLOGY

In order to achieve the objectives of this research it is essential to have a good understanding of several topics such as hydraulic fracturing, fracture geometry models and shale gas characteristics. This has been accomplished by research and study of several credible sources of the related topics that can be found in the references.

Based on the results of the research, a two-dimensional hydraulic fracture geometry model has been selected that is most suitable in the design of a hydraulic fracture treatment for shale gas reservoirs. It must be noted that due to time constraints and also for simplicity, only the two-dimensional models are studied and used in this research. The selected 2D model and the selection's reasoning are fully explained in the results and discussion section (chapter 4). Additionally, two mathematical computer codes were developed by using Matlab. The first code was developed based on the PKN-C model in order to investigate the effect of several parameters used in the model. And the second mathematical code was developed based on the KGD-C model as a means of parameter sensitivity comparison between the two models. The mathematical computer codes are discussed in more detail in section 3.2. At the final stage of this study, the effect of various parameters, such as fluid loss, rock stiffness and fracture height on the fracture geometry is analyzed.

3.1 Gantt Chart

Please refer to APPENDIX I.

3.2 Methodology Flow Chart

The flow chart of this study is presented in Figure 3.1.

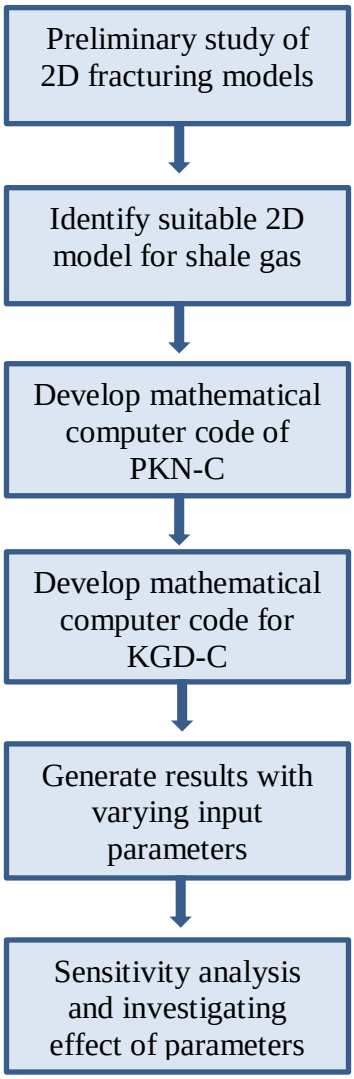

Figure 3.1 Methodology flow chart

3.3 Mathematical Computer Code of PKN-C Model

In order to produce results based on the PKN-C model, a mathematical computer code is developed by using Matlab. This mathematical code will include two different modes known as the Design mode and the Simulation mode.

3.3.1 Design Mode

In the Design mode several parameters are given to the program to generate the Maximum fracture width at wellbore, average fracture width, wellbore net pressure and the pumping time. Table 1 shows the input and output parameters of the design mode:

Table 1. Input and output parameters in the PKN-C design mode.

Input Parameters		Output Parameters	
h_f	Fracture Height	$w_{w,0}$	Maximum Fracture Width at Wellbore
C_L	Leak Off Coefficient	$\overline{w}$	Average Fracture Width
S_p	Spurt Loss	t	Pumping Time
E'	Plane Strain Modulus	$p_{n,w}$	Wellbore Net Pressure
μ	Fluid Viscosity		
i	Injection Rate		
x_f	Fracture Length		

The code calculates the Wellbore width and fracture width based on the input parameters and by using the following two equation:

Maximum fracture width at wellbore: $$w_{w,0} = 3.27\left(\frac{\mu i x_f}{E'}\right)^{1/4} \quad \textbf{(2.1)}$$

Average fracture width: $$\overline{w} = \frac{\pi}{5} w_{w,0} = 2.05\left(\frac{\mu i x_f}{E'}\right)^{1/4} \quad \textbf{(2.2)}$$

Moreover the pumping time is calculated for a given fracture length using the PKN fracture length equation:

$$x_f = \frac{(\overline{w} + 2S_p)i}{4C_L{}^2 \pi h_f}\left[\exp(\beta^2)erfc(\beta) + \frac{2\beta}{\sqrt{\pi}} - 1\right] \qquad \textbf{(2.4)}$$

And finally the wellbore net pressure for the given fracture length and width is calculated:

$$p_{n,w} = \frac{E'}{2h_f} w_{w,0} \qquad \textbf{(2.6)}$$

In this mode multiple values of each parameter from an excel spreadsheet are given into the program as input while multiple results are generated and stored in a table format for further analysis. Additionally, the code produces several curves by plotting various input and output parameters (Figure 3.2).

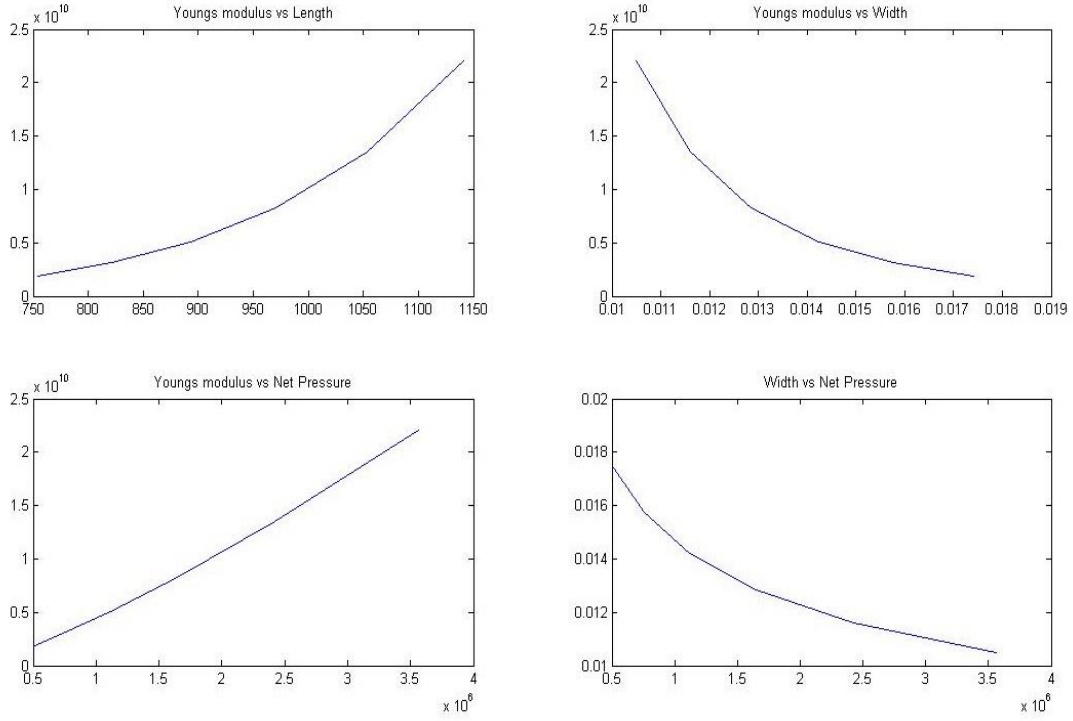

Figure 3.2 Graphs generated by Matlab code

3.3.2 Simulation Mode

The Simulation mode is similar to the design mode while the difference is in the desired output. In the simulation mode the fracture length, maximum wellbore width,

average fracture width, and the net wellbore pressure is calculated based on a given pumping time (Table 2).

Table 2. Input and output parameters in PKN-C simulatione mode.

Input Parameters		Output Parameters	
h_f	Fracture Height	$w_{w,0}$	Maximum Fracture Width at Wellbore
C_L	Leak Off Coefficient	$\overline{w}$	Average Fracture Width
S_p	Spurt Loss	x_f	Fracture Length
E	Plane Strain Modulus	$p_{n,w}$	Wellbore Net Pressure
μ	Fluid Viscosity		
i	Injection Rate		
t	Pumping Time		

3.4 Mathematical Computer Code for KGD-C Model

In addition to the PKN-C model, a mathematical computer code of the KGD-C model is also developed in two modes (Design and Simulation) to enable comparison of the predicted values in each model while analyzing the effect of different parameters in this project. Additionally, the KGD-C code is used as an aid to justify the selection of the PKN-C model.

The mathematical code of the KGD-C model has the same input and out parameters as the PKN-C model. However, the code uses the following two equations to calculate the fracture width at the well bore and the average fracture width:

Fracture Width at Wellbore: $$w_w = 3.22\left(\frac{\mu i x_f^{\,2}}{h_f E'}\right)^{1/4} \quad \textbf{(3.1)}$$

Average Fracture Width: $$\overline{w} = 2.53\left(\frac{\mu i x_f^{\,2}}{h_f E'}\right)^{1/4} \quad \textbf{(3.2)}$$

And finally, the following equation is used to calculate the wellbore net pressure:

$$p_{n,w} = \frac{E'}{4x_f} w_w \quad \textbf{(3.3)}$$

CHAPTER 4

RESULTS AND DISCUSSION

4.1 Selecting The 2D Model

The two most commonly used hydraulic fracture geometry models in the oil and gas industry are the PKN and KGD model. However, according to Rahman et al. (2010), the PKN-C model is most favored in the Petroleum industry. This model uses the Carter II solution of material balance with a constant injection rate and considers the fluid leak-off. The PKN-C model is favored mostly due to assuming a vertical plane strain in this model, which is more suitable for a fracture with a fixed height, where the fracture's length is significantly larger than its height (Valko et al., 1995).

Moreover, other researchers such as Holditch et al. (1995) argue that fracture lengths predicted by the PKN-C model are nearer to the values estimated by three-dimensional models when compared to other 2D models.

Smrecak (2011), argues that the stiffness of the rock has a great influence on the rock's fracture geometry. A stiff rock, such as shale, has a high stress to strain ratio (high modulus), and generally the fracture growth in such rocks is longer and narrower compared to the fracture growth in soft formations in which fractures are wide and short. According to Smrecak (2011), this is because in soft formations "the pressures causing the fractures can penetrate and dissipate further laterally (into planes of weakness like bedding planes and existing fractures) within the rock unit." This is further illustrated in the following figures which were generated based on the results produced by the Matlab code. Figure 4.1 indicates increase of fracture propagation in the rock as the modulus increases, while Figure 4.2 indicates the reduction in fracture width as the modulus increases.

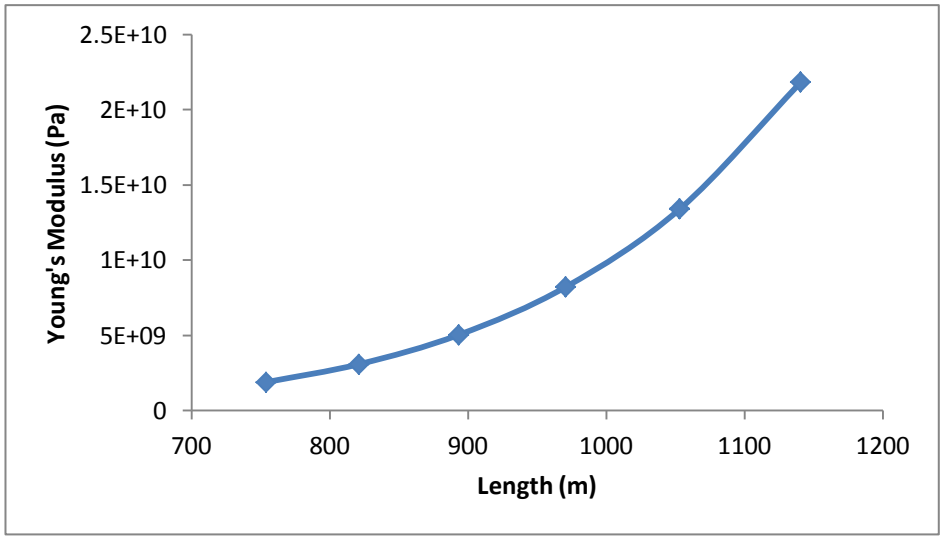

Figure 4.1 Effect of young's modulus on fracture length

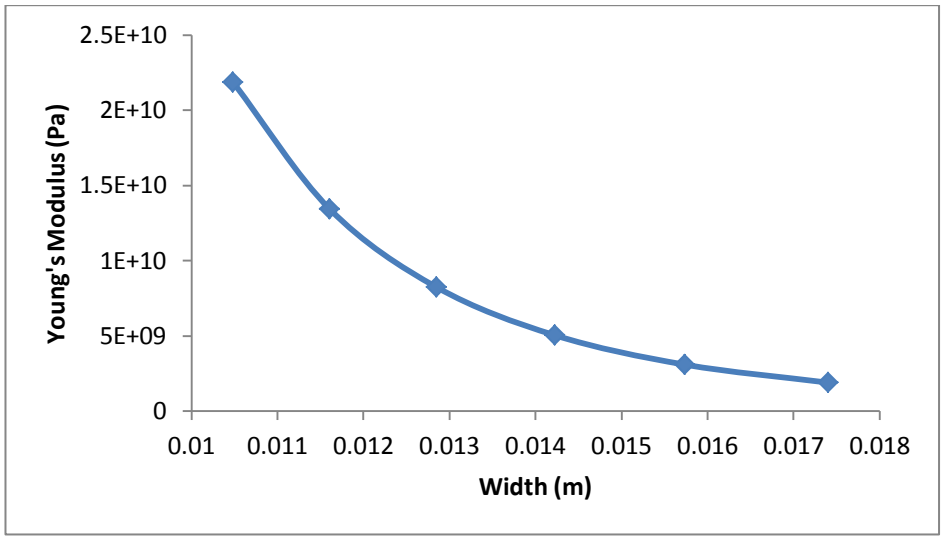

Figure 4.2 Effect of young's modulus on fracture width.

Moreover, while comparing the two most common 2D models in the industry, KGD and PKN, it is observed that the KGD model predicts wider and shorter fractures due to assuming the plane strain in the horizontal direction, while the PKN model predicts longer and narrower fractures as it assumes the plane strain in the vertical direction (Syed, 2010; Allen & Roberts, 1989). The effects of the horizontal and vertical plane strain assumptions in these two models on the predicted fracture lengths and width are illustrated in the Figures 4.3 and 4.4.

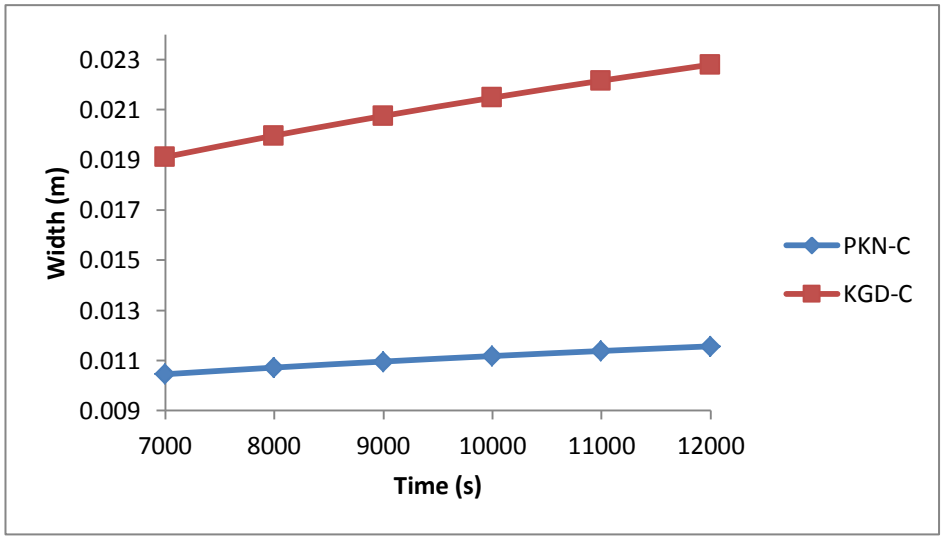

Figure 4.3 Fracture widths predicted by PKN-C and KGD-C models.

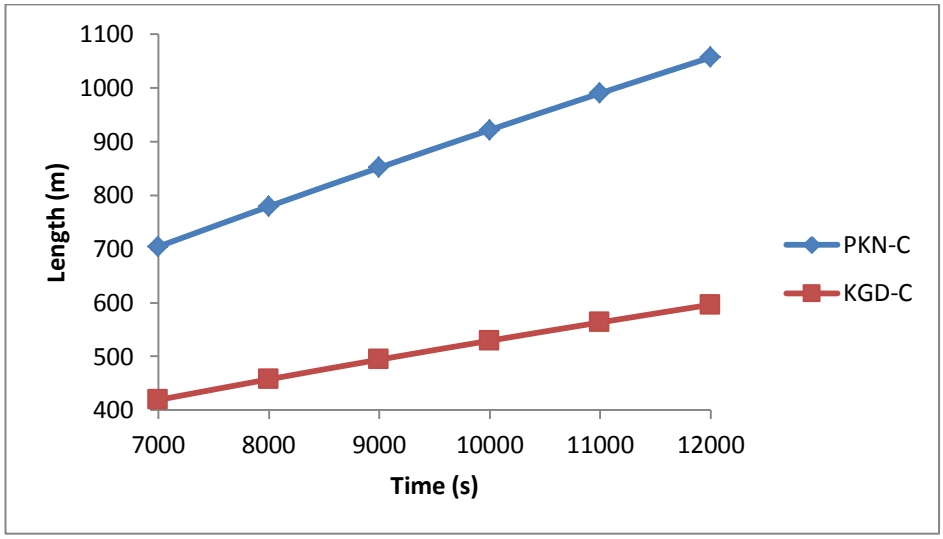

Figure 4.4 Fracture lengths predicted by PKN-C and KGD-C models

Figure 4.3 indicates that with the same input parameters used for both models, the PKN-C model predicts narrower fractures compared to the KGD-C model, while Figure 4.4 illustrates the shorter fractures predicted by the KGD-C model.

Additionally, according to Mohanty (2009), low permeability formations such as shale reservoirs require narrower and longer fractures for a higher productivity. Thus, using a model that would result in longer and narrower fractures, such as the PKN-C model, would be more suitable for shale formations which are extremely low in permeability.

4.2 Effect of Fracture Height on Length

As shown in Figure 4.5 and 4.6, fracture length and fracture width are plotted against injection time for two given fracture heights. It is observed that assuming a greater fracture height results in shorter and narrower fractures at any given injection time while considering a fixed injection rate. It is noticeable that increasing the fracture height from 40 m to 80 m has reduced the fracture length to almost half of its value at any given time, which indicates that fracture length is an almost linear and a strong function of fracture height. Thus, it is important to have a correct estimate of the fracture height in two dimensional models, due to the high sensitivity of the fracture geometry to variation in fracture height.

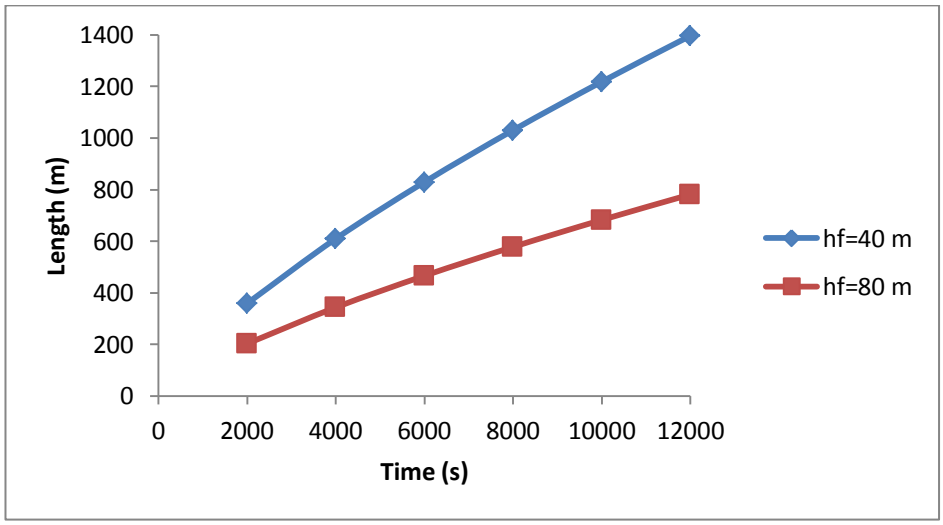

Figure 4.5 Effect of fracture height on fracture propagation.

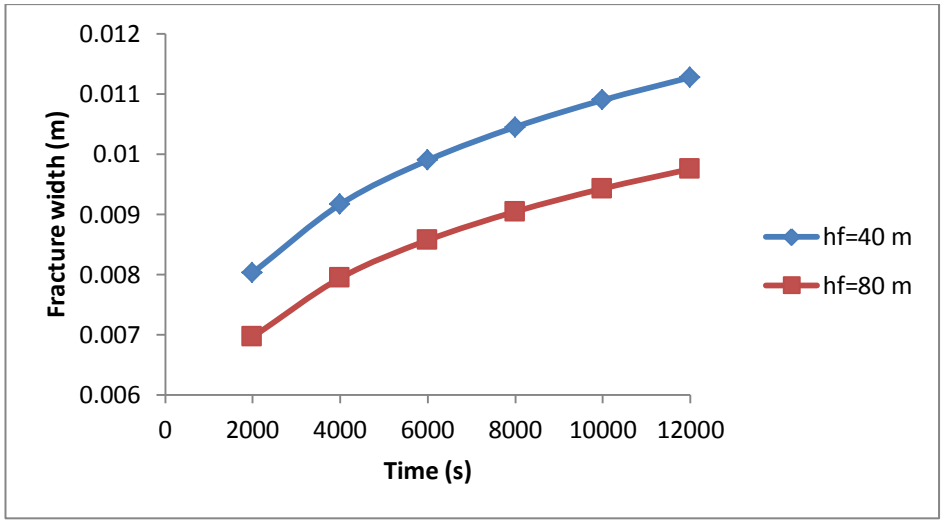

Figure 4.6 Effect of fracture height on fracture width

As mentioned, a greater fracture height will result in lower fracture length and width values at a constant injection rate. This is because considering a larger fracture height will require larger volumes of fluid to be injected in order to maintain a high pressure to produce a fracture with desired length and width (Fisher, 2012). This can be observed in Figure 4.7 where fracture length is plotted against the injected fluid volume.

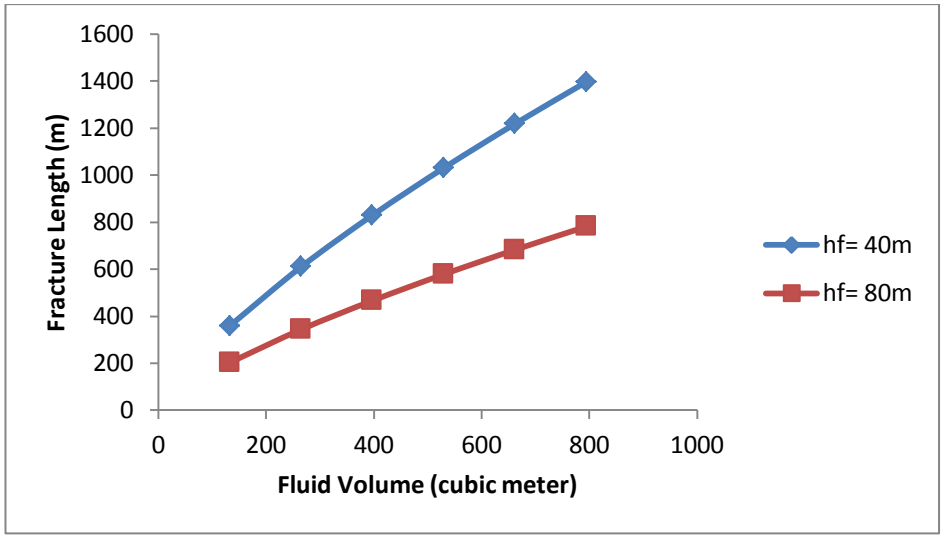

Figure 4.7 Fracture lenght and Fliud volume

4.3 Effect of Fluid Leak off on Length

In Figure 4.8 the effect of fluid leak off on fracture penetration is illustrated, where fracture length is plotted against time for two leak off coefficients.

It is observed that a higher leak off coefficient results in shorter fracture lengths at any given time. This is because more fluid is leaking off into the formation which causes a lower build-up pressure for further fracture propagation (Newman, 2009). However, the effect of leak off coefficient on the length is not as significant as the effect of fracture height. This can be observed while increasing the leak off coefficient from 9.84E-6 to 1.96E-5 $m/s^{0.5}$ (100% increase) results in a decrease in fracture length by less than 20%.

.

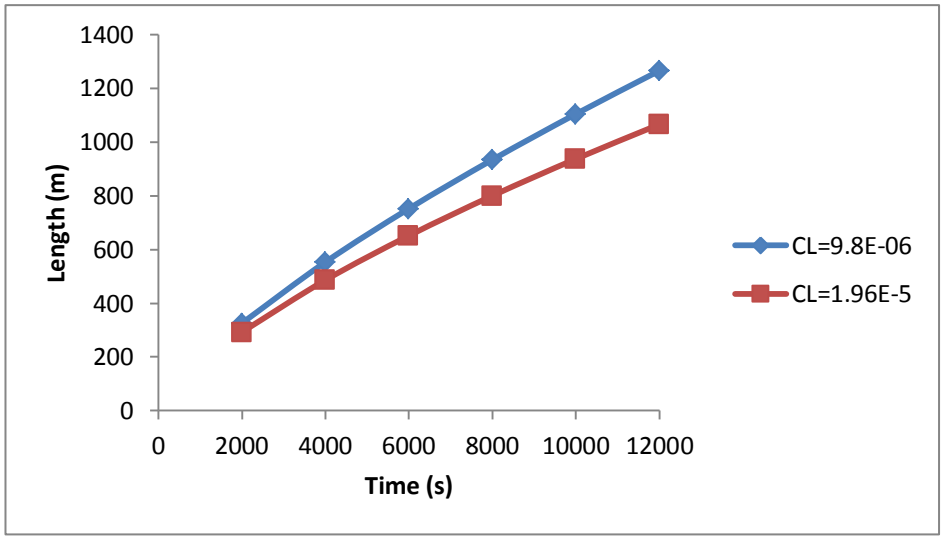

Figure 4.8 Effect of fluid loss on fracture propagation.

However, this is not the case if we are dealing with higher fluid losses. At higher leak off coefficients we can observer an almost linear relationship between the length and leak off coefficient. In Figure 4.9 it is observed that by doubling the leak off coefficient the fracture length reduces by almost 50% at any given time.

Thus, it can be concluded that fracture length is more sensitive towards the fracture height compared to fluid loss, unless the fluid loss rates are high.

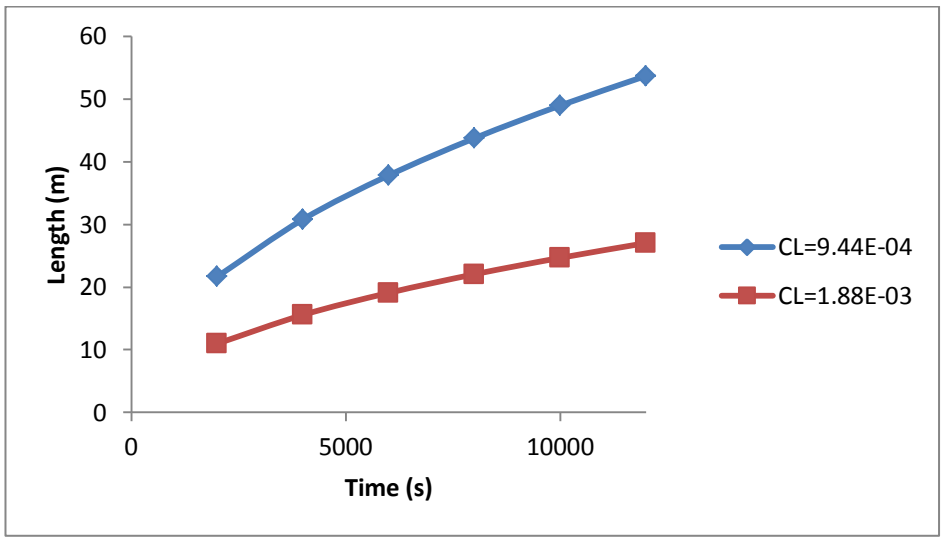

Figure 4.9 Effect of high fluid losses on fracture propagation.

4.4 Effect of Fracture Height on Fluid Efficiency

In Figure 4.10 fluid efficiency, which represents the fraction of injection fluid that remains in the fracture, is plotted against time. It is observed that fluid efficiency decreases with time. This is due to the fact that as injection time, and consequently the fracture length increase, the fracture surface area is increasing. And with increasing injection time and surface area, more fluid is leaked off in to the formation.

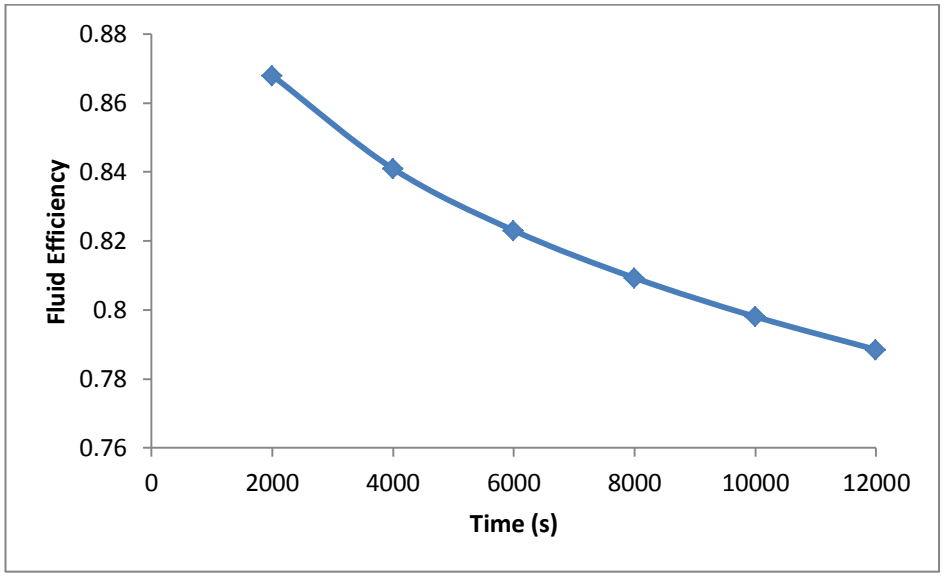

Figure 4.10 Fluid efficiency decreasing with time and length.

This can also be observed in Figure 4.11 which indicates a decrease in efficiency as the fracture length grows. It is also observed that a greater fracture height will result in lower fluid efficiency at a given length. Again this is due to the increase in fracture surface area which results in higher fluid leak off.

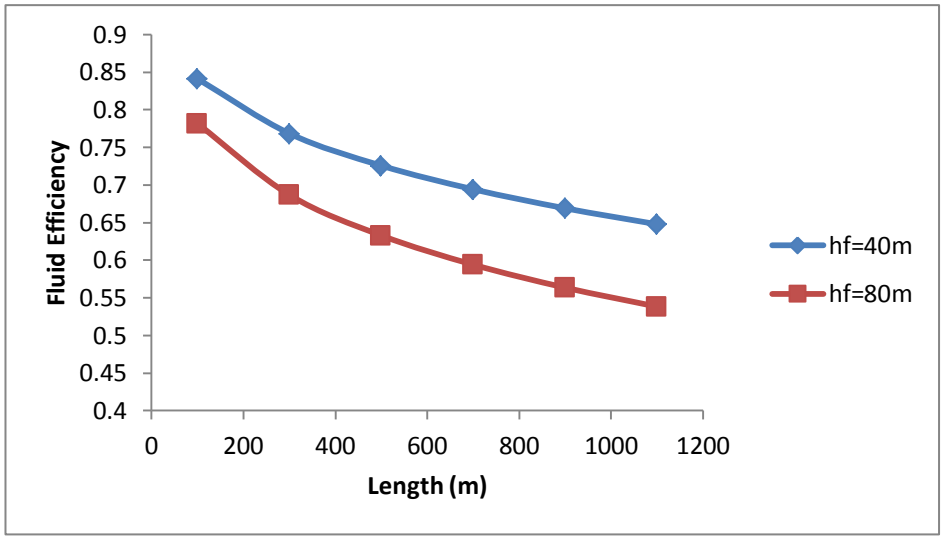

Figure 4.11 Effect of fracture height on fluid efficiency

4.5 Fracture Conductivity and Folds of Increase

Two factors influence the productivity of wells that are hydraulically fractured. The first is the fracture's capacity to receive formation fluid, which is influenced by the fracture geometry, and the second factor is the ability of the fracture to carry the formation fluid to the wellbore which is influenced by the fracture permeability, K_f (Guo et al., 2007). Moreover, Rahman et al. (2010), argues that the importance of fracture conductivity is not limited to productivity, but is also important in terms of fracturing fluid recovery. Soliman and Hunt, 1985 (as stated by Rahman et al., 2010), further explain that a higher fracture conductivity might be required to clean-up the fracture, compared to the optimum fracture conductivity for producing from the reservoir. The dimensionless fracture conductivity is defined as (Cinco-Ley and Samaniego,1981):

$$F_{CD} = \frac{K_f w}{K x_f} \qquad \textbf{(4.1)}$$

Where F_{CD} is the dimensionless fracture conductivity, $K_f w$ is the fracture conductivity, K and K_f are the reservoir and fracture permeability, respectively.

In 1961, Prats suggested that (as cited by Economides et al., 1989), there is a relationship between the length and width of a fracture in order to reach maximum productivity, which can be expressed by the dimensionless fracture conductivity

concept. Prats argued that for any fracture volume, when F_{CD} is equal to 1.3 (or close to this value), maximum productivity would be achieved. However, according to Economides et al. (1989), the optimum F_{CD} value suggested by Prats would only be suitable for reservoirs with high permeabilities, and the value 1.3 is an order of magnitude lower than the optimum F_{CD} to achieve maximum productivity in reservoirs with extremely low permeabilities. Furthermore, for a reservoir with low permeability, in which long fractures are produced, an optimum dimensionless conductivity equal to 10 is commonly used. (NSI Technologies, Inc., 2001)

In Figure 4.12 the dimensionless fracture conductivity is plotted against injection time. It can be observed that the F_{CD} is decreasing as injection time increases. This is reasonable due to the fact that the fracture length increases with time and F_{CD} is inversely proportional to the fracture length. . The graph also indicates higher F_{CD} values predicted by the KGD-C model compared to the PKN-C model. This again is justified based on the shorter fracture lengths that are predicted by the KGD-C model.

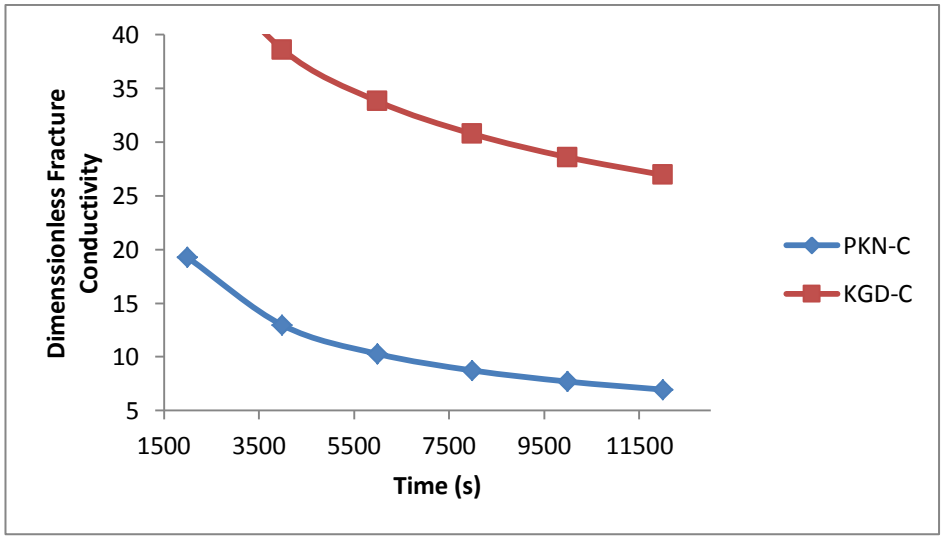

Figure 4.12 Fcd decreasing with time and higher dimensionless conductivity predicted by KGD-C model.

It is also observed that a much longer injection time will be required to reach the optimum value of F_{CD} =10 in the KGD-C model in comparison to the PKN-C model

which reaches the optimum dimensionless fracture conductivity in just over 6000 seconds (100 minutes).

The input data used in the above calculations, and the entire study, are hypothetical and were selected based on ranges of values provided by various authors. Please see Appendix II, III and IV for data range values of shale permeability, common young's modulus values and Poisson's ratio in shale formations.

The reservoir and well data used for calculations are presented in Table 3.

Table 3. Reservoir and well data.

Parameter	value	Parameter	Value
Wellbore radius	**0,10668 m**	**Leak-off coefficient**	**9.84E − 6 m/s$^{0.5}$**
Drainage radius	**914.4 m**	**Spurt loss**	**0**
Reservoir permeability	**0.1 md**	**Skin factor**	**0**
Fracture permeability	**80 d**	**Injection Rate**	**0.0662 m^3/s**
Young's modulus	**2.0E10 Pa**	**Fracture height**	**45 m**
Poisson's ratio	**0.1**	**Fluid Viscosity**	**0.2 Pa.s**

With the help of the dimensionless fracture conductivity concept and folds of increase, the stimulation results can be measured in terms of productivity. Economides et al., (1989), defines folds of increase (FOI) as the increase in productivity of the well after the hydraulic fracture treatment compared with the well's productivity before treatment. FOI can be calculated from:

$$FOI = \frac{\ln(r_e / r_w) + s}{\ln(r_e / r'_w)} \qquad \textbf{(4.2)}$$

Where r_e is the reservoir drainage radius, r_w is the wellbore radius, r'_w is the equivalent wellbore radius and s is the pre-fracture skin. The equivalent wellbore radius, r'_w, can be calculated using Figure 4.13 developed by Cinco-Ley (NSI Technologies, Inc., 2001):

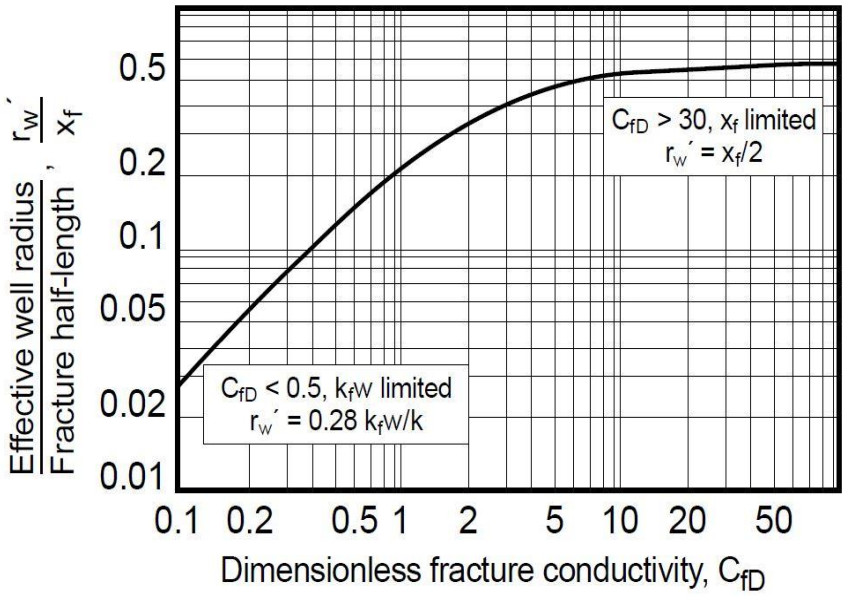

Figure 4.13 Calculating rw' as a function of Fcd after Cinco-Ley . Adapted from *Reservoir Stimulation* (p. 5-12), by M. J. Economides and K. G. Nolte, 1989, Houston, TX: Schlumberger Educational Services.

In Figures 4.14 and 4.15 the folds of increase is plotted against the injection time and fracture length. It is observed that the FOI increases with time. This indicates that as time increases, and the fracture propagates further into the reservoir, higher productivity is achieved.

As shown, the fracture geometry predicted by the PKN-C model results in higher post-fracture productivity compared to KGD-C model. In the PKN-C model, it is observed that at an optimum condition of F_{CD}=10, the folds of increase is equal to almost 11 at an injection time just over 6000 seconds (100 minutes) and a fracture length of almost 780 meters. On the other hand, while comparing the two models, it is observed that the KGD-C fracture geometry results in lower well productivity, and would require more than 200 minutes of injection time to achieve FOS=11.

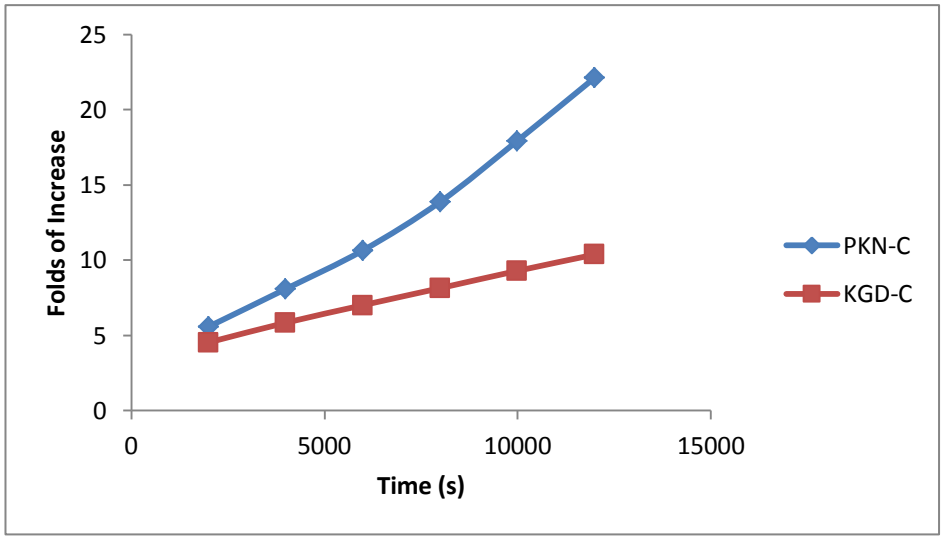

Figure 4.14 Increase in productivity with time.

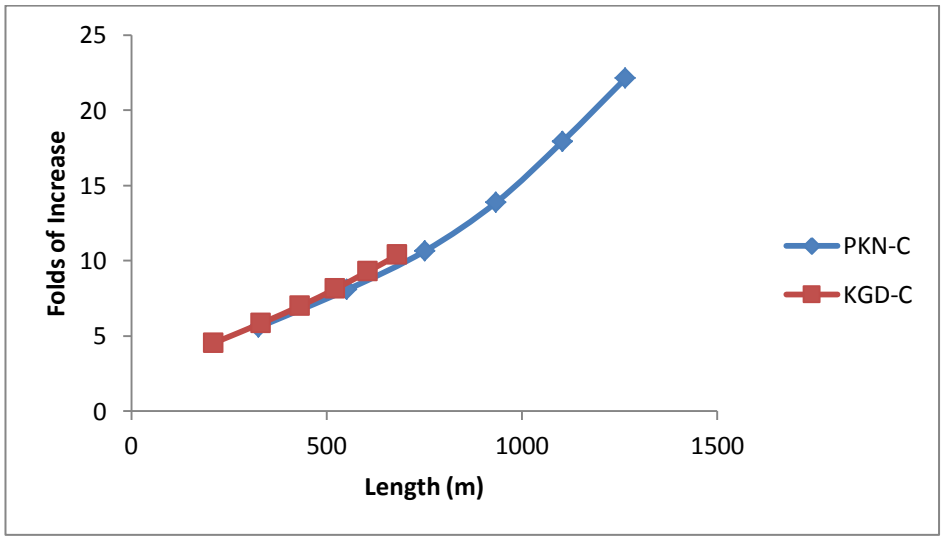

Figure 4.15 Higher folds of increase in PKN-C model.

CHAPTER 5

CONCLUSION

In this study, various hydraulic fracture geometry models were studied and their application in unconventional formations was investigated. Furthermore, the two most commonly used hydraulic fracture geometry models in the oil and gas industry, PKN and KGD, have been discussed.

Based on the results of the preliminary research, a two-dimensional hydraulic fracture geometry model was identified that would be most suitable to be used in the design of a hydraulic fracture treatment for shale gas reservoirs. PKN-C is the selected model as several researchers and literature suggest that the assumptions in this model are more acceptable while it also predicts more accurate fracture lengths in comparison with other two-dimensional models. Parameters predicted by the PKN-C model and a second 2D model, KGD-C, were compared and analyzed to justify the model selection and to investigate the effect of various parameters on the fracture geometry and the well.

Moreover, based on the PKN-C and KGD-C models, two mathematical computer codes were developed in order to calculate various parameters such as fracture length, average fracture width, wellbore net pressure, pumping time, and maximum fracture width at wellbore.

5.1 Summary of Results

- Longer and narrower fractures are produced in rocks with a higher Young's modulus (such as shale), when all other input parameters are kept unchanged.

- Wider and shorter fractures are produced in rocks with a lower Young's modulus, when all other input parameters are kept unchanged.
- The PKN-C model predicts longer and narrower fractures compared to the KGD-C model when all input parameters are kept unchanged.
- Low permeability formations such as shale reservoirs require narrower and longer fractures for a higher productivity. Thus, using a model that would predict longer and narrower fractures, such as the PKN-C model, would be more suitable for shale formations which are extremely low in permeability.
- Assuming a greater fracture height results in a shorter and narrower fracture at a constant injection rate and injection time, when all other parameters are kept unchanged.
- An Increase in the leak off coefficient when fluid loss is small will result in slightly shorter fracture lengths, when all other parameters are kept unchanged.
- An increase in the leak off coefficients when fluid loss is significant will result in significantly shorter fracture lengths and an almost linear relationship between the length and leak off coefficient is observed.
- The fracture surface area increases with pumping time and fracture length, causing more fluid leaking off into the formation and resulting in lower fluid efficiency.
- Assuming a greater fracture height will result in a lower fluid efficiency at any given fracture length as a result of increase in fracture surface area.
- The dimensionless fracture conductivity decreases as injection time increases when all other input parameters are kept unchanged. This is because the fracture length increases with time and dimensionless fracture conductivity is inversely proportional to the fracture length.
- The KGD-C model predicts a higher dimensionless fracture conductivity compared to the PKN-C model at a constant injection rate and time, due to the shorter fractures predicted in the KGD-C model.
- A much longer injection time is required to reach the optimum value of dimensionless fracture conductivity in the KGD-C model in comparison to the PKN-C model.

- As injection time increases, and the fracture propagates further into the reservoir, FOI is increased and higher productivity is achieved.
- The fracture geometry predicted by the PKN-C model results in higher post-fracture productivity compared to KGD-C model when all conditions kept unchanged.

5.2 Future Work

- Develop a laboratory experimental setup to investigate the effect of various parameters on the fracture geometry and compare with the results obtained from the PKN-C model.

REFERENCES

Gomaa, A. M. Qi Qu, Maharidge, R., Nelson, S., and Reed, T., 2014. *New Insights into Hydraulic Fracturing of Shale Formations*, Presented at the International Petroleum Technology Conference 2014, IPTC 2014, IPTC 17594, Doha, Qatar January 20-22, 2014.

Valko, P., and Economides, M. J. 1995. Hydraulic Fracture Mechanics. Chichester, England: John Wiley & Sons.

American Petroleum Institute. (2013, October). *Shale Energy: 10 Points everyone should know.* Retrieved February 5, 2014, from API.org: http://www.api.org/~/media/Files/Policy/Hydraulic_Fracturing/Hydraulic-Fracturing-10-points.pdf

Economides, M. J., and Nolte, K. G. 1989. Reservoir Stimulation, Second edition. Houston, TX: Schlumberger Educational Services.

Guo, B., Lyons, W., & Ghalambor, A. (2007). *Petroleum production engineering* (1st ed.). Burlington, MA: Gulf Professional Pub.

Nolen-Hoeksema, R. (2013). Elements of Hydraulic Fracturing. *Oilfield Review, 25*(2), 51.

Geertsma, J. 1989. *Two-Dimensional Fracture-Propagation Models.* In: Recent Advances in Hydraulic Fracturing, Monograph Vol. 12, Gidley, J. L. et al. (Eds.). Richardson, TX: SPE.

Xiang, J. 2011. *A PKN Hydraulic Fracture Model Study and Formation Permeability Determination*, MS thesis, Texas A&M University, College Station, TX.

Rahman, M. M. and Rahman, K. K. 2010. *A Review of Hydraulic Fracture Models and Development of an Improved Pseudo-3D Model for Stimulating Tight Oil/Gas Sand.* Energy Sources, Part A 32:1416–1436.

Smrecak, T. A., & PRI Marcellus Shale Team, 2011. *Jointing and Fracturing in the Marcellus Shale.* The Marcellus Papers, August 2011 (5). Retrieved from: http://cce.cornell.edu/EnergyClimateChange/NaturalGasDev/Documents/PRI%20Papers/Marcellus_issue5.pdf.

Syed, A. H. 2010. *Fracture initiation and propagation in poroelastic medium and investigation of potential for introducing a secondary fracture treatment*, MS thesis, University of New South Wales, Australia.

Allen, T. O., & Roberts, A. P. 1989. *Production Operations, Well Completions, Workover, and Stimulation* (3rd ed.). Tulsa: Oil & Gas Consultants International.

Mohanty, K. K., 2009. *Improvement of Fracturing in Gas Shales, Technology Status Assessment*. Retrieved from: http://www.rpsea.org/media/files/project/91bafd02/07122-38-TS-Improvement_Fracturing_Gas_Shales-05-26-09_P.pdf.

Fisher, M., & Warpinski, N. (2012). *Hydraulic-Fracture-Height Growth: Real Data*. SPE Production & Operations, 27(01), 8-19. doi:10.2118/145949-PA

Newman, M. S., Pavloudis, M., & Rahman, M. M. 2009. *Importance of Fracture Geometry and Conductivity in Improving Efficiency of Acid Fracturing in Carbonates*. Presented at the Canadian International Petroleum Conference, Paper 2009-146. Calgary, Canada.

Cinco-Ley, H., & Samaniego-V., F. (1981). Transient Pressure Analysis for Fractured Wells. *Journal of Petroleum Technology*, 33(09), 1749–1766.

NSI Technologies. Inc. (2001). *Optimum Fracture Design*. NSI Technologies Frac Tips, 3 (1). Retrieved from http://www.nsitech.com/wp-content/uploads/2014/06/nsi_fractip_optimumfracture.pdf

Clark, C., Burnham, A., Harto, C., and Horner, R., 2013, *Hydraulic Fracturing and Shale Gas Production: Technology, Impacts, and Regulations*, ANL/EVS/R-12/5, Argonne National Laboratory, Argonne, IL.

Amadei, B. (n.d). Lecter Note 5: *Deformability Properties of Rocks and Masses*, Retrieved from: http://ceae.colorado.edu/~amadei/CVEN5768/PDF/NOTES5.pdf

Total S.A. (n.d). *Three Main Sources Of Unconventional Gas*. Retreived from: http://www.total.com/en/energies-expertise/oil-gas/exploration-production/strategic-sectors/unconventional-gas/presentation/three-main-sources-unconventional-gas.

APPENDIX

APPENDIX 1: Gantt Chart

- The following chart illustrates the timeline and key milestones of the project during FYP I

No.	Detail	1	2	3	4	5	6	7	8	9	10	11	12	13	14
1	Selection of Project Topic		•												
2	Preliminary Research Work														
3	Submission of Extended Proposal						•								
4	Proposal Defense								•	•					
7	Submission of Interim Report														•

No.	Detail	1	2	3	4	5	6	7	8	9	10	11	12	13	14
1	Preliminary Research Work & Studying various models	■	■	■	■	■	■	■	■	■	■				
2	Selection of 2D model											■			
3	Selection of Parameters												■	■	
4	Start work on computer code													■	■

Table 4 Gantt Chart FYP I

- The following chart illustrates the timeline and key milestones of the project during FYP II.

No.	Detail	1	2	3	4	5	6	7	8	9	10	11	12	13	14
2	Submission of progress report							•							
6	Submission of Dissertation												•		
7	Submission of Technical Paper												•		
8	Viva													•	
9	Submission of Project Dissertation														•

No.	Detail	1	2	3	4	5	6	7	8	9	10	11	12	13	14
1	Develop a computer code	■	■	■	■										
2	Investigate effect of Parameters					■	■	■	■	■	■				
3	Conclude Results										■	■			

Table 5 Gantt Chart FYP II

APPENDIX II: Young's Modulus for Various Rocks

Table 6. Range of Young's modulus for various rocks. Adapted from *Deformability Properties of Rocks and Masses*, by B. Amadei (n.d).

	Granite	Basalt	Gneiss	Schist	Quart-zite	Marble	Lime-stone	Sand-stone	Shale
Av. E	59.3	62.6	58.6	42.4	70.9	46.3	50.4	15.3	13.7
Max. E	75.5	100.6	81.0	76.9	100.0	72.4	91.6	39.2	21.9
Min. E	26.2	34.9	16.8	5.9	42.4	23.2	7.7	1.9	7.5
Range	49.3	65.7	64.2	71.0	57.6	49.2	83.9	37.3	14.4
No. of samples	24	16	17	18	10	16	29	18	9

APPENDIX III: Poisson's Ratio for Various Rocks

Table 7. Range of Poisson's Ratio for various rocks. Adapted from *Deformability Properties of Rocks and Masses,* by B. Amadei (n.d)

	Granite	Basalt	Gneiss	Schist	Quart-zite	Marble	Lime-stone	Sand-stone	Shale
Av. ν	0.23	0.25	0.21	0.12	0.15	0.23	0.25	0.24	0.08
Max. ν	0.39	0.38	0.40	0.27	0.24	0.40	0.33	0.46	0.18
Min. ν	0.10	0.16	0.08	0.01	0.07	0.10	0.12	0.06	0.03
Range	0.29	0.22	0.32	0.26	0.17	0.30	0.21	0.40	0.15
No. of samples	24	16	17	18	10	16	29	18	9

APPENDIX IV: Permeability of Different types of Gas Reservoirs

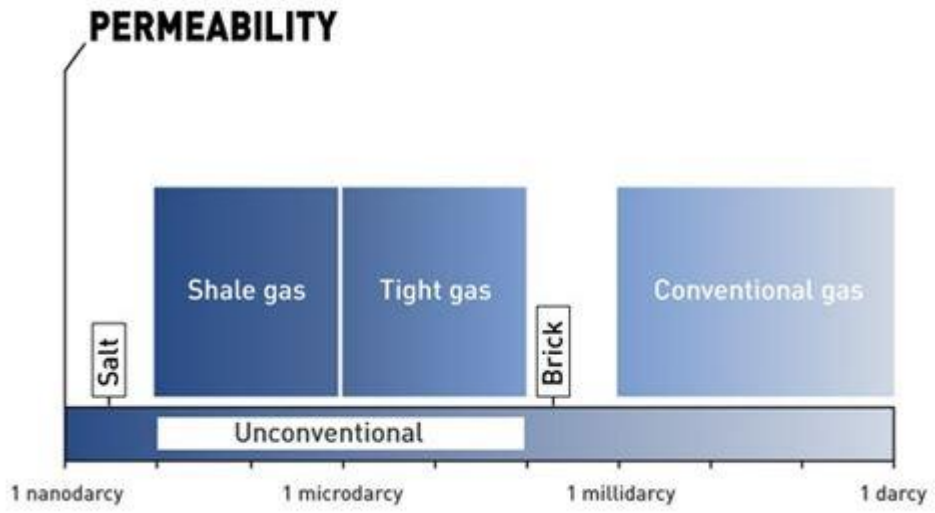

Figure A1 Permeability for different types of gas reservoir. Adapted from *Three Main Sources Of Unconventional Gas*, by Total S.A. (n.d)

APPENDIX V: Mathematical Computer Code for PKN-C Design Mode

```
% read from excel file
filename = 'myExample.xlsx';
% CL = first col
% Sp = second col
% hf = third col
% dE = forth col
% mu = fifth col
% i = sixth col
% xf = seventh col
data = xlsread(filename);

[EW, tsolved , W_W0, P_nw] = myfun(data(:,1),data(:,2),data(:,3),data(:,4),data(:,5),data(:,6),data(:,7));

results = [EW,tsolved,W_W0,P_nw];
Names_var =  {'EW'; 't'; 'W_W0';'P_nw'};

%write data in csv format
fid = fopen('results_April_15-2014.csv','w');
fprintf(fid, [Names_var{1} sprintf(',%s',Names_var{2:end}) '\n']);
fclose(fid)
dlmwrite('results_April_15-2014.csv', results, '-append', ...
        'delimiter', ',','precision','%.10f');
```

```
function [EW, tsolved , W_W0, P_nw] = myfun(CL,Sp,hf,dE,mu,i,xf)

 EW = 2.05*((mu.*i.*xf)./dE).^0.25;

n = size(CL,1);
tsolved = zeros(n,1);
for k = 1:n
syms t
tsolved(k) = solve(xf(k) == ((EW(k)+2*Sp(k))*i(k))/(4*CL(k)^2*pi*hf(k))*...
        (exp((2*CL(k)*sqrt(pi*t)/(EW(k)+2*Sp(k)))^2 )*erfc((2*CL(k)*sqrt(pi*t))/(EW(k)+2*Sp(k)))+...
        (2*(2*CL(k)*sqrt(pi*t))/(EW(k)+2*Sp(k)))/(sqrt(pi))-1),t);
end

W_W0 = 3.27*((mu.*i.*xf)./dE).^0.25;
P_nw = (dE./(2.*hf)).*W_W0;

figure;
subplot(2,2,1)
plot(mu,EW)
title('mu vs EW')
subplot(2,2,2)
plot(mu,P_nw)
title('mu vs pressure')
subplot(2,2,3)
plot(P_nw,EW)
title('P vs width ')
subplot(2,2,4)
plot(P_nw,EW)
title('P vs xf')

end
```

APPENDIX VI: Mathematical Computer Code for PKN-C Simulation Mode

```
% read from excel file
filename = 'myExamplexf.xlsx';
data = xlsread(filename);
[EW, xfsolved , W_W0, P_nw] = myfun_xf(data(:,1),data(:,2),data(:,3),data(:,4),data(:,5),data(:,6),data(:,7));
results = [EW,xfsolved,W_W0,P_nw];
Names_var =  {'EW'; 'xf'; 'W_W0';'P_nw'};

%write data in csv format
fid = fopen('Results_xf.csv','w');
fprintf(fid, [Names_var{1} sprintf(',%s',Names_var{2:end}) '\n']);
fclose(fid)
dlmwrite('Results_xf.csv', results, '-append', ...
        'delimiter', ',','precision','%.10f');
```

```
function [EW, xfsolved , W_W0, P_nw] = myfun_xf(CL,Sp,hf,dE,mu,i,t)

n = size(CL,1);
xfsolved = zeros(n,1);
EW = zeros(n,1);

for k = 1:n
syms xf EW

[xfsolved(k), EW(k)] = solve(xf == ((EW+2*Sp(k))*i(k))/(4*CL(k)^2*pi*hf(k))*...
        (exp((2*CL(k)*sqrt(pi*t(k))/(EW+2*Sp(k)))^2 )*erfc((2*CL(k)*sqrt(pi*t(k)))/(EW+2*Sp(k)))+...
        (2*(2*CL(k)*sqrt(pi*t(k)))/(EW+2*Sp(k)))/(sqrt(pi))-1),EW == 2.05*((mu(k).*i(k).*xf)./dE(k)).^0.25, xf,
EW);

EW = 2.05*((mu.*i.*xfsolved)./dE).^0.25;
W_W0 = 3.27*((mu.*i.*xfsolved)./dE).^0.25;
P_nw = (dE./(2.*hf)).*W_W0;
end

figure;
subplot(2,2,1)
plot(xfsolved,dE)
title('dE vs length')
subplot(2,2,2)
plot(EW,dE)
title('dE vs width')
subplot(2,2,3)
plot(xfsolved,t)
title('xf vs t')
subplot(2,2,4)
plot(hf,t)
title('hf vs t')
 end
```

APPENDIX VII: Mathematical Computer Code for KGD-C Design Mode

```
% read from excel file
filename = 'myExamplekgd.xlsx';
data = xlsread(filename);

[EW, tsolved , W_W0, P_nw] = myfunkgd(data(:,1),data(:,2),data(:,3),data(:,4),data(:,5),data(:,6),data(:,7));
 results = [EW,tsolved,W_W0,P_nw];
Names_var =  {'EW'; 't'; 'W_W0';'P_nw'};

%write data in csv format
fid = fopen('KGD_results.csv','w');
fprintf(fid, [Names_var{1} sprintf(',%s',Names_var{2:end}) '\n']);
fclose(fid)
dlmwrite('KGD_results.csv', results, '-append', ...
        'delimiter', ',','precision','%.10f');
```

```
function [EW, tsolved , W_W0, P_nw] = myfunkgd(CL,Sp,hf,dE,mu,i,xf)

 EW = 2.53*((mu.*i.*xf.^2)./(hf.*dE)).^0.25;

n = size(CL,1);
tsolved = zeros(n,1);
for k = 1:n
syms t
tsolved(k) = solve(xf(k) == ((EW(k)+2*Sp(k))*i(k))/(4*CL(k)^2*pi*hf(k))*...
        (exp((2*CL(k)*sqrt(pi*t)/(EW(k)+2*Sp(k)))^2 )*erfc((2*CL(k)*sqrt(pi*t))/(EW(k)+2*Sp(k)))+...
        (2*(2*CL(k)*sqrt(pi*t))/(EW(k)+2*Sp(k)))/(sqrt(pi))-1),t);
end

W_W0 = 3.22*((mu.*i.*xf.^2)./(hf.*dE)).^0.25;
P_nw = (dE./(4.*xf)).*W_W0;

figure;
subplot(2,2,1)
plot(mu,EW)
title('mu vs EW')
subplot(2,2,2)
plot(mu,P_nw)
title('mu vs pressure')
subplot(2,2,3)
plot(P_nw,EW)
title('P vs width ')
subplot(2,2,4)
plot(P_nw,EW)
title('P vs xf')

 end
```

APPENDIX VIII: Mathematical Computer Code for KGD-C Simulation Mode

```
% read from excel file
filename = 'myExamplexfkgd.xlsx';
data = xlsread(filename);

[EW, xfsolved , W_W0, P_nw] = myfun_xfkgd(data(:,1),data(:,2),data(:,3),data(:,4),data(:,5),data(:,6),data(:,7));
 results = [EW,xfsolved,W_W0,P_nw];
Names_var =  {'EW'; 'xf'; 'W_W0';'P_nw'};

%write data in csv format
fid = fopen('Results_xf_KGD.csv','w');
fprintf(fid, [Names_var{1} sprintf(',%s',Names_var{2:end}) '\n']);
fclose(fid)
dlmwrite('Results_xf_KGD.csv', results, '-append', ...
      'delimiter', ',','precision','%.10f');
```

```
function [EW, xfsolved , W_W0, P_nw] = myfun_xfkgd(CL,Sp,hf,dE,mu,i,t)

n = size(CL,1);
xfsolved = zeros(n,1);
EW = zeros(n,1);

for k = 1:n
syms xf EW

[xfsolved(k), EW(k)] = solve(xf == ((EW+2*Sp(k))*i(k))/(4*CL(k)^2*pi*hf(k))*...
      (exp((2*CL(k)*sqrt(pi*t(k))/(EW+2*Sp(k)))^2 )*erfc((2*CL(k)*sqrt(pi*t(k)))/(EW+2*Sp(k)))+...
      (2*(2*CL(k)*sqrt(pi*t(k)))/(EW+2*Sp(k)))/(sqrt(pi))-1),EW ==
2.53*((mu(k).*i(k).*xf.^2)./(hf(k).*dE(k))).^0.25, xf, EW);

EW = 2.53*((mu.*i.*xfsolved.^2)./(hf.*dE)).^0.25;
W_W0 = 3.22*((mu.*i.*xfsolved.^2)./(hf.*dE)).^0.25;
P_nw = (dE./(4.*xfsolved)).*W_W0;
end

 figure;
subplot(2,2,1)
plot(xfsolved,dE)
title('dE vs length')
subplot(2,2,2)
plot(EW,dE)
title('dE vs width')
subplot(2,2,3)
plot(xfsolved,t)
title('xf vs t')
subplot(2,2,4)
plot(hf,t)
title('hf vs t')
 end
```

APPENDIX IX: Input and output parameters for examining effect of rock stiffness on length and width

Table 8. Input and out parameters for examining effect of rock stiffness

C_L m/s$^{0.5}$	S_p m	h_f m	E Pa	μ Pa.s	i m^3/s	t s	ν -	E' Pa	$\overline{w}$ m	x_f m	$w_{w,0}$ m	$p_{n,w}$ Pa
9.84E-06	0	51.8	1.9E+09	0.2	0.0662	12000	0.1	1.92E+09	0.01741	754.1381	0.027772	514471.7
9.84E-06	0	51.8	3.1E+09	0.2	0.0662	12000	0.1	3.13E+09	0.015741	821.3662	0.025109	758182.4
9.84E-06	0	51.8	5.05E+09	0.2	0.0662	12000	0.1	5.1E+09	0.014228	893.5399	0.022695	1117014
9.84E-06	0	51.8	8.23E+09	0.2	0.0662	12000	0.1	8.31E+09	0.012856	970.8199	0.020506	1645150
9.84E-06	0	51.8	1.34E+10	0.2	0.0662	12000	0.1	1.35E+10	0.011612	1053.331	0.018522	2422160
9.84E-06	0	51.8	2.19E+10	0.2	0.0662	12000	0.1	2.21E+10	0.010484	1141.152	0.016724	3564825

APPENDIX X: Input and out parameters for KGD-C and PKN-C width and length comparison

Table 9. Input and out parameters for KGD-C and PKN-C width and length comparison

C_L m/s$^{0.5}$	S_p m	h_f m	μ Pa.s	i m^3/s	t s	E' Pa	$\overline{w}$ m		x_f m	
							PKN-C	KGD-C	PKN-C	KGD-C
9.84E-06	0	51.8	0.2	0.0662	7000	1.38E+10	0.010455	0.019115	704.4876	419.2515
9.84E-06	0	51.8	0.2	0.0662	8000	1.38E+10	0.010721	0.019968	779.1449	457.5349
9.84E-06	0	51.8	0.2	0.0662	9000	1.38E+10	0.010962	0.020753	851.377	494.1799
9.84E-06	0	51.8	0.2	0.0662	10000	1.38E+10	0.011181	0.02148	921.5048	529.4272
9.84E-06	0	51.8	0.2	0.0662	11000	1.38E+10	0.011382	0.02216	989.779	563.4618
9.84E-06	0	51.8	0.2	0.0662	12000	1.38E+10	0.011569	0.022799	1056.401	596.4298

APPENDIX XI: Input and out parameters for investigating effect of height

Table 10. Input and out parameters for investigating effect of height on length

C_L m/s$^{0.5}$	S_p m	h_f m	μ Pa.s	i m^3/s	t s	E' Pa	$\overline{w}$ m	x_f m	$w_{w,0}$ m	$p_{n,w}$ Pa
Fracture height = 40 m										
9.84E-06	0	40	0.2	0.0662	2000	2.02E+10	0.008029	358.9752	0.012807	3234015
9.84E-06	0	40	0.2	0.0662	4000	2.02E+10	0.009166	609.7376	0.01462	3691999
9.84E-06	0	40	0.2	0.0662	6000	2.02E+10	0.009898	829.2668	0.015789	3987029
9.84E-06	0	40	0.2	0.0662	8000	2.02E+10	0.01045	1030.219	0.016669	4209284
9.84E-06	0	40	0.2	0.0662	10000	2.02E+10	0.010897	1218.157	0.017382	4389365
9.84E-06	0	40	0.2	0.0662	12000	2.02E+10	0.011275	1396.187	0.017985	4541630
Fracture height = 80 m										
9.84E-06	0	80	0.2	0.0662	2000	2.02E+10	0.006962	202.9138	0.011104	1402083
9.84E-06	0	80	0.2	0.0662	4000	2.02E+10	0.007941	343.4848	0.012666	1599274
9.84E-06	0	80	0.2	0.0662	6000	2.02E+10	0.00857	466.083	0.013671	1726083
9.84E-06	0	80	0.2	0.0662	8000	2.02E+10	0.009044	578.0025	0.014426	1821496
9.84E-06	0	80	0.2	0.0662	10000	2.02E+10	0.009427	682.4479	0.015038	1898730
9.84E-06	0	80	0.2	0.0662	12000	2.02E+10	0.009751	781.2081	0.015555	1963982

APPENDIX XII: Input and out parameters for investigating effect of Leak off

Table 11. Input and out parameters for investigating effect of Leak off on length

C_L m/s$^{0.5}$	S_p m	h_f m	μ Pa.s	i m^3/s	t s	E' Pa	$\overline{w}$ m	x_f m	$w_{w,0}$ m	$p_{n,w}$ Pa
$C_L = 0.000944$										
0.000944	0	45	0.2	0.0662	2000	2.02E+10	0.003979	21.66034	0.006347	1424753
0.000944	0	45	0.2	0.0662	4000	2.02E+10	0.004345	30.79618	0.006931	1555778
0.000944	0	45	0.2	0.0662	6000	2.02E+10	0.004574	37.81351	0.007296	1637703
0.000944	0	45	0.2	0.0662	8000	2.02E+10	0.004743	43.73259	0.007566	1698340
0.000944	0	45	0.2	0.0662	10000	2.02E+10	0.004879	48.94927	0.007782	1746867
0.000944	0	45	0.2	0.0662	12000	2.02E+10	0.004992	53.66672	0.007963	1787515
$C_L = 0.001888$										
0.001888	0	45	0.2	0.0662	2000	2.02E+10	0.003357	10.97793	0.005356	1202136
0.001888	0	45	0.2	0.0662	4000	2.02E+10	0.003663	15.56034	0.005844	1311681
0.001888	0	45	0.2	0.0662	6000	2.02E+10	0.003855	19.07799	0.006149	1380246
0.001888	0	45	0.2	0.0662	8000	2.02E+10	0.003997	22.04416	0.006375	1431023
0.001888	0	45	0.2	0.0662	10000	2.02E+10	0.00411	24.65779	0.006556	1471675
0.001888	0	45	0.2	0.0662	12000	2.02E+10	0.004205	27.02094	0.006708	1505735

APPENDIX XIII: Input and out parameters for calculating Dimensionless fracture conductivity and Folds of increase

Table 12. Input and out parameters for calculating Dimensionless fracture conductivity and Folds of increase

C_L m/s$^{0.5}$	S_p m	h_f m	μ Pa.s	i m^3/s	t s	E' Pa	$\overline{w}$ m		x_f m		F_{CD} -		FOI -	
							PKN-C	KGD-C	PKN-C	KGD-C	PKN-C	KGD-C	PKN-C	KGD-C
9.84E-06	0	45	0.2	0.0662	2000	2.02E+10	0.007837	0.012764	325.8576	210.9161	19.23961	48.41454	5.588189	4.540717
9.84E-06	0	45	0.2	0.0662	4000	2.02E+10	0.008945	0.016024	553.1803	332.4045	12.93651	38.56534	8.094771	5.850029
9.84E-06	0	45	0.2	0.0662	6000	2.02E+10	0.009659	0.018301	752.0675	433.5689	10.27483	33.76771	10.66226	7.015166
9.84E-06	0	45	0.2	0.0662	8000	2.02E+10	0.010197	0.020108	934.0443	523.4154	8.733565	30.73318	13.88797	8.149347
9.84E-06	0	45	0.2	0.0662	10000	2.02E+10	0.010633	0.02163	1104.176	605.6707	7.703507	28.57014	17.94866	9.297453
9.84E-06	0	45	0.2	0.0662	12000	2.02E+10	0.011001	0.022958	1265.291	682.3331	6.955437	26.91736	22.13253	10.37877